

Multivariable Predictive Control of Thin Film Deposition Using a Stochastic PDE Model

Dong Ni and Panagiotis D. Christofides*

Department of Chemical Engineering, University of California, Los Angeles, California 90095-1592

In this work, we focus on a thin film deposition process which takes place on a two-dimensional (2D) lattice and is governed by three microscopic processes including molecule adsorption, surface migration, and desorption. A 2D linear stochastic partial differential equation (PDE) model is initially constructed which describes the spatio-temporal evolution of the film surface. Then, the control problem is formulated as the one of regulating the thin film thickness and surface roughness by manipulating the substrate temperature and adsorption rate. Subsequently, a computationally efficient multivariable predictive control algorithm is developed which uses a finite-dimensional approximation of the stochastic PDE model to regulate the thin film thickness and surface roughness at desired levels at the end of the deposition. The predictive controller is then applied to the kinetic Monte Carlo simulation of the deposition process. Closed-loop system simulation results demonstrate that the model is adequately accurate and that the controller is effective in enforcing the desired control objectives and reducing film variance.

1. Introduction

Thin films of advanced materials are used in a wide range of applications, e.g., microelectronic devices, optics, microelectromechanical systems (MEMS), and biomedical products. Various deposition methods have been developed and widely used to prepare thin films such as physical vapor deposition (PVD) and chemical vapor deposition (CVD). However, the dependence of the thin film properties, such as uniformity, composition, and microstructure, on the deposition conditions is a serious constraint on reproducing thin film's performance.

Operating thin film deposition under real-time feedback control is one way of meeting the increasingly stringent requirements on the quality of thin films and reducing thin film variability. Motivated by this, earlier research efforts focused on feedback control of thin film deposition processes with emphasis on deposition spatial uniformity control (see refs 1 and 2 for results on rapid thermal processing (RTP) and ref 3 on plasma-enhanced chemical vapor deposition (PECVD)) and on thin film composition control (see ref 4 for experimental results on real-time carbon content control in a PECVD process). More recently, there has been significant attention on feedback control of thin film microstructure arising from the need to produce thin films with well-defined microstructure. In a thin film growth process, the film is directly shaped by microscopic random processes (e.g., molecule adsorption, desorption, migration, and surface reaction). Models that describe these microscopic processes and directly account for their stochastic nature are needed for precise control of film microstructure. Examples of such models include (1) kinetic Monte Carlo (kMC) methods^{5–6} and (2) stochastic partial differential equations (PDEs).^{8,9}

Methodologies for estimation-based feedback control and model-predictive control using kinetic Monte Carlo models have recently been developed in refs 10–12 and

13, respectively. However, the fact that kMC models are not available in closed-form makes it very difficult to use them for system-level analysis and the design and implementation of real-time model-based feedback control systems. Based on the fact that kinetic Monte Carlo simulations provide realizations of a stochastic process which are consistent with the master equation that describes the evolution of the microscopic probability distribution, a method to construct reduced-order approximations of the master equation was reported in ref 14. Furthermore, an approach was also reported in refs 15 and 16 to identify linear deterministic models from outputs of kinetic Monte Carlo simulators and design controllers using linear control theory. This approach is effective in controlling macroscopic variables which are low statistical moments of the microscopic distributions (e.g., surface coverage, which is the zeroth moment of adspecies distribution on a lattice). However, to control higher statistical moments of the microscopic distributions, such as the surface roughness (the second moment of height distribution on a lattice) or even the microscopic configuration (such as the surface morphology), deterministic models may not be sufficient. This is because the effect of the stochastic nature of the microscopic processes becomes very significant in these cases and must be addressed in both the model construction and controller design.

Stochastic PDE models, on the other hand, which are available in closed-form, have been developed to describe the evolution of the height profile for surfaces in certain physical and chemical processes such as epitaxial growth⁹ and ion sputtering.¹⁷ More recently, Lou and Christofides presented a method for feedback control of surface roughness in a thin film growth process using one-dimensional (1D) stochastic PDE models.^{18,19} Pole-placement controller design was carried out directly based on the stochastic PDE models which describe the surface height fluctuation, and the feedback controller was successfully applied to the kMC model of the process regulating the surface roughness to desired values in deposition¹⁸ and sputtering¹⁹ processes.

* To whom correspondence should be addressed. Tel.: 310-794-1015. Fax: 310-206-4107. E-mail: pdc@seas.ucla.edu.

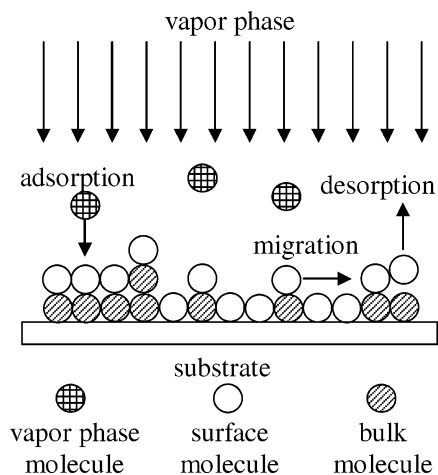


Figure 1. The thin film growth process.

However, the construction of stochastic PDE models for thin film growth processes directly based on microscopic process rules^{20–22} is a very difficult task. The lack of a systematic approach to construct stochastic PDE models has prohibited the development of stochastic PDE models, and subsequently the design of feedback control systems. Motivated by this, we proposed, in our recent work,²³ a systematic method to construct stochastic PDE models for thin film growth using first-principles-based microscopic simulations. The method was applied to a representative deposition process, and a 1D linear stochastic PDE model was constructed. This model was successfully validated through simulations and was subsequently used to design a model-based feedback controller to regulate the surface roughness.

In this work, we focus on a thin film deposition process which takes place on a two-dimensional (2D) lattice and is governed by three microscopic processes including molecule adsorption, surface migration, and desorption. A 2D linear stochastic PDE model is initially constructed, following the methodology proposed in our previous work,²³ which describes the spatio-temporal evolution of the film surface. Then, the control problem is formulated as the one of regulating the thin film thickness and surface roughness by manipulating the substrate temperature and adsorption rate. Subsequently, a computationally efficient multivariable predictive control algorithm is developed which uses a finite-dimensional approximation of the stochastic PDE model to regulate the thin film thickness and surface roughness at desired levels at the end of the deposition. The predictive controller is then applied to the kMC simulation of the deposition process. Closed-loop system simulation results demonstrate that the model is adequately accurate and that the controller is effective in enforcing the desired control objectives and reducing film variance.

2. Preliminaries

2.1. Thin Film Growth Process. In this work, we consider a thin film growth process of deposition from vapor phase, in which the formation of the thin film is governed by three microscopic processes that occur on the surface as shown in Figure 1, i.e., the adsorption of vapor phase molecules on the surface, the migration of surface molecules, and the desorption of surface molecules. This process is, in fact, a very common thin film

growth process that can be traced in most chemical vapor deposition processes.

More specifically, we consider a single species growth on a 2D lattice. The adsorption rate which depends on the vapor phase concentration is considered uniform over the spatial domain. All surface sites are available for adsorption for all time, and the adsorption rate for each surface site is denoted as W (expressed in number of molecules adsorbed per second, 1/s).

The migration rate of each surface molecule depends on its local environment. Under the consideration of only first nearest-neighbor interactions, the migration rate of surface molecules from a surface site with n first nearest-neighbors is given by

$$w_m(n) = k_{m0} e^{-(E_s + nE_n)/k_B T} \quad (1)$$

where E_s is the energy barrier associated with migration due to surface effects, E_n is the energy barrier associated with migration due to nearest-neighbor interactions, k_{m0} is the frequency constant associated with migration, k_B is the Boltzmann's constant, and T is the substrate temperature. The values of migration energy barriers and frequency constant used in this study are taken from the literature²⁴ for a molecular beam epitaxy GaAs process and are as follows: $E_s = 1.58$ eV, $E_n = 0.28$ eV, and $k_{m0} = 2k_B T/h$, where h is Planck's constant.

The desorption rate of each surface molecule also depends on its local environment. Under the consideration of only first nearest-neighbor interactions, the desorption rate of surface molecules from a surface site with n first nearest-neighbors is given by

$$w_d(n) = k_{d0} e^{-(E_d + nE_n)/k_B T} \quad (2)$$

where E_d is the energy barrier associated with desorption due to surface binding, and k_{d0} is the frequency constant associated with desorption. We use the values $E_d = 1.8$ eV and $k_{d0} = 2k_B T/h$ in this work.

A kinetic Monte Carlo simulation code following the algorithm reported in ref 25 is used to simulate the deposition process and obtain surface snapshots. First, the surface molecules are grouped into three classes based on the number of first nearest neighbors (from 0 to 4 neighbors); in each class, the molecules have the same migration rate and desorption rate, and the adsorption rate is site independent. Then, a random number is generated to select an event to be executed based on the rates; if the event is migration or desorption, the class in which the event will occur is also selected. After that, a second random number is generated to select the site where the event will be executed; if the event is adsorption, the site is randomly picked among all the sites in the entire lattice; if the event is migration or desorption, the site is randomly picked from the list of the sites in the selected class. After the site is selected, the Monte Carlo event is executed. If the event is adsorption, it is executed by adding one molecule on the selected site; if the event is migration, the molecule on the site is moved to one of the vacant neighboring sites with equal probability; if the event is desorption, it is executed by removing the top molecule on the selected site. Upon an executed event, a time increment τ is added to the process time t , computed based on the following equation (see ref 5 for a detailed proof):

$$\tau = - \frac{\ln \zeta}{Wk_{\max}^2 + \sum_{n=0}^4 N_n [w_m(n) + w_d(n)]} \quad (3)$$

where ζ is a random number that follows the uniform distribution in the unit interval, N_n is the number of surface molecules with n first nearest-neighbors, and k_{\max} is the size of the simulation lattice (i.e., the total number of surface sites is k_{\max}^2). Furthermore, periodic boundary conditions are used in the kMC simulation to satisfy the mass balance of the migration of the surface molecules.

2.2. Stochastic PDE Model. We now proceed with constructing a closed-form stochastic PDE model using the approach we developed in ref 23. Without any a priori knowledge of the deposition process, we assume that there exists a 2D linear stochastic PDE of the following general form that can adequately describe the evolution of the surface of the thin film during the deposition:

$$\frac{\partial h}{\partial t} = c + c_1 \nabla h + c_2 \nabla^2 h + \dots + c_w \nabla^w h + \xi(x, y, t) \quad (4)$$

where $x \in [0, \pi]$, $y \in [0, \pi]$ is the spatial coordinate, t is the time, $h(x, y, t)$ is the height (in the unit of monolayers (ML)) of the surface at position x, y , and time t , and $\xi(x, y, t)$ is a Gaussian noise with zero mean and covariance:

$$\langle \xi(x, y, t) \xi(x', y', t') \rangle = \zeta^2 \delta(x - x') \delta(y - y') \delta(t - t') \quad (5)$$

where $\delta(\cdot)$ is the Dirac function. Furthermore, the prederivative coefficients c and c_j in eq 4 and the parameter ζ^2 in eq 5 depend on the process parameters, the substrate temperature T , and adsorption rate W (directly determined by vapor phase concentration):

$$\begin{aligned} c &= C[T(t), W(t)] \\ \zeta^2 &= C_\xi[T(t), W(t)] \\ c_j &= C_j[T(t), W(t)] \quad j = 0, \dots, w \end{aligned} \quad (6)$$

where $C(\cdot)$ and $C_j(\cdot)$ are nonlinear functions to be determined.

The stochastic PDE of eq 4 is subjected to the following periodic boundary conditions:

$$\begin{aligned} \nabla^j h(0, y, t) &= \nabla^j h(\pi, y, t) \\ \nabla^j h(x, 0, t) &= \nabla^j h(x, \pi, t) \quad j = 0, \dots, w - 1 \end{aligned} \quad (7)$$

and the initial condition

$$h(x, y, 0) = h_0(x, y) \quad (8)$$

Remark 1. In this work, we assume that a linear stochastic PDE model should adequately describe the process dynamics; however, for the cases in which the nonlinear dynamics are significant, nonlinear stochastic PDE models would be needed. Also, we note that we use a scalar function, $h(\cdot)$, to represent the height profile of the thin film surface in the model. In general, $h(\cdot)$ can be a vector function and be used to represent any appropriate microscopic description of the thin film (such as the defect locations, grain boundaries, etc.); in

such a case, several stochastic PDEs should be considered simultaneously.

To study the dynamics of eq 4, we initially consider the eigenvalue problem of the linear operator of eq 4, which takes the form

$$\begin{aligned} A\phi_{m,n}(x, y) &= c_1 \nabla \phi_{m,n}(x, y) + c_2 \nabla^2 \phi_{m,n}(x, y) + \dots + \\ &\quad c_w \nabla^w \phi_{m,n}(x, y) \\ &= \lambda_{m,n} \phi_{m,n}(x, y) \\ \nabla^j \phi_{m,n}(0, y) &= \nabla^j \phi_{m,n}(\pi, y) \\ \nabla^j \phi_{m,n}(x, 0) &= \nabla^j \phi_{m,n}(x, \pi) \quad j = 0, \dots, w - 1 \\ &\quad m, n = 0, \pm 1, \dots, \pm \infty \end{aligned} \quad (9)$$

where $\lambda_{m,n}$ denotes the eigenvalue and $\phi_{m,n}$ denotes the eigenfunction. A direct computation of the solution of the above eigenvalue problem yields

$$\begin{aligned} \lambda_{m,n} &= (I2m + I2n)c_1 + [(I2m)^2 + (I2n)^2]c_2 + \dots + \\ &\quad [(I2m)^w + (I2n)^w]c_w \\ \phi_{m,n}(x, y) &= \frac{1}{\pi} (e^{I2mx + I2ny}) \quad m, n = 0, \pm 1, \dots, \pm \infty \end{aligned} \quad (10)$$

where $\lambda_{m,n}$ denotes the (m, n) th eigenvalue, $\phi_{m,n}(x, y)$ denotes the (m, n) th eigenfunction, and $I = \sqrt{-1}$.

To present the method that we use for parameter identification of the stochastic PDE of eq 4, we first derive an infinite stochastic ordinary differential equation (ODE) representation of eq 4 using modal decomposition and parametrize the infinite stochastic ODE system using kMC simulation. We first expand the solution of eq 4 in an infinite series in terms of the eigenfunctions of the operator of eq 9 as follows (i.e., the Fourier expansion in the complex form):

$$h(x, y, t) = \sum_{m,n=-\infty}^{\infty} z_{m,n}(t) \phi_{m,n}(x, y) \quad (11)$$

where $z_{m,n}(t)$ are time-varying coefficients. Substituting the above expansion for the solution, $h(x, y, t)$, into eq 4 and taking the inner product, the following system of infinite stochastic ODEs is obtained:

$$\frac{dz_{m,n}}{dt} = \lambda_{m,n} z_{m,n} + c_{m,n}^z + \xi_{m,n}(t) \quad m, n = 0, \pm 1, \dots, \pm \infty \quad (12)$$

with the initial conditions

$$z_{m,n}(0) = z_{m,n,0} \quad m, n = 0, \pm 1, \dots, \pm \infty \quad (13)$$

where $c_{m,n}^z = c \int_0^\pi \int_0^\pi \phi_{m,n}^*(x, y) dx dy$, $\xi_{m,n}(t) = \int_0^\pi \int_0^\pi \xi(x, y, t) \phi_{m,n}^*(x, y) dx dy$, and $z_{m,n,0} = \int_0^\pi \int_0^\pi h_0(x, y) \phi_{m,n}^*(x, y) dx dy$. Apparently, $c_{0,0}^z = \pi c$ and $c_{m,n}^z = 0$ when $m^2 + n^2 \neq 0$. $\phi_{m,n}^*$ is the complex conjugate of $\phi_{m,n}$; the superscript star is used to denote complex conjugate in the remainder of this manuscript.

The covariance of $\xi_{m,n}(t)$ can be computed by using the following result:²⁶

Result 1. If (1) $f(x)$ is a deterministic function, (2) $\eta(x)$ is a random variable with $\langle \eta(x) \rangle = 0$ and covariance $\langle \eta(x) \eta^*(x') \rangle = \sigma^2 \delta(x - x')$, and (3) $\epsilon = \int_a^b f(x) \eta(x) dx$, then

ϵ is a random number with $\langle \epsilon \rangle = 0$ and covariance $\langle \epsilon \epsilon^* \rangle = \sigma^2 \int_a^b f(x) f^*(x) dx$.

Using result 1, we obtain $\langle \xi_{m,n}(t) \rangle = 0$ and $\langle \xi_{m,n}(t) \xi_{m,n}^*(t') \rangle = \zeta^2 \delta(t - t')$. We note that $\xi_{m,n}(t)$ is a complex Gaussian random variable.

To parametrize this infinite stochastic ODE system, we first derive the analytic expressions for the statistical moments of the stochastic ODE states, such as the expected values and covariances. By comparing the analytical expression to the statistical moments obtained by multiple kMC simulations, the parameters of the stochastic ODE system (i.e., $\lambda_{m,n}$ and ζ) can be determined.

The analytic solution to eq 12 is obtained as follows to derive the expressions for the statistical moments of the stochastic ODE states:

$$z_{m,n}(t) = e^{\lambda_{m,n}t} z_{m,n,0} + \frac{(e^{\lambda_{m,n}t} - 1) c_{m,n}^z}{\lambda_{m,n}} + \int_0^t e^{\lambda_{m,n}(t-\mu)} \xi_{m,n}(\mu) d\mu \quad (14)$$

Using result 1, eq 14 can be further simplified as follows:

$$z_{m,n}(t) = e^{\lambda_{m,n}t} z_{m,n,0} + \frac{(e^{\lambda_{m,n}t} - 1) c_{m,n}^z}{\lambda_{m,n}} + \theta_{m,n}(t) \quad (15)$$

where $\theta_{m,n}(t)$ is a complex random variable of normal distribution with zero mean and covariance

$$\langle \theta_{m,n}(t) \theta_{m,n}^*(t) \rangle = \zeta^2 \frac{e^{(\lambda_{m,n} + \lambda_{m,n}^*)t} - 1}{\lambda_{m,n} + \lambda_{m,n}^*}$$

Therefore, the first stochastic moment (the expected value) and the second stochastic moment (the covariance) of state $z_{m,n}$ can be expressed as follows:

$$\langle z_{m,n}(t) \rangle = e^{\lambda_{m,n}t} z_{m,n,0} + \frac{(e^{\lambda_{m,n}t} - 1) c_{m,n}^z}{\lambda_{m,n}}$$

$$\langle z_{m,n}(t) z_{m,n}^*(t) \rangle = \zeta^2 \frac{e^{(\lambda_{m,n} + \lambda_{m,n}^*)t} - 1}{\lambda_{m,n} + \lambda_{m,n}^*} + \langle z_{m,n}(t) \rangle \langle z_{m,n}(t) \rangle^* \quad (16)$$

Remark 2. We note that eqs 14–16 hold for all stochastic ODE states. Particularly, when $m = n = 0$ (i.e., for state $z_{0,0}$), $\lambda_{m,n} = 0$, these terms in the equations with $\lambda_{m,n}$ and $\lambda_{m,n} + \lambda_{m,n}^*$ as denominators should be calculated as follows:

$$\lim_{\lambda_{m,n} \rightarrow 0} \frac{(e^{\lambda_{m,n}t} - 1) c_{m,n}^z}{\lambda_{m,n}} = t c_{m,n}^z$$

$$\lim_{\lambda_{m,n} \rightarrow 0} \zeta^2 \frac{e^{(\lambda_{m,n} + \lambda_{m,n}^*)t} - 1}{\lambda_{m,n} + \lambda_{m,n}^*} = \zeta^2 t$$

Eq 16 holds for any initial condition $z_{m,n,0}$. Since we are able to choose any initial thin film surface profile for simulation, we choose $z_{m,n,0} = 0$ (i.e., the initial surface is flat, $h(x, y, 0) = 0$) to simplify our calculations. In this case, eq 16 can be further simplified as follows (note that $c_{m,n}^z = 0, \forall m^2 + n^2 \neq 0$):

$$\langle z_{m,n}(t) \rangle = 0$$

$$\langle z_{m,n}(t) z_{m,n}^*(t) \rangle = \zeta^2 \frac{e^{(\lambda_{m,n} + \lambda_{m,n}^*)t} - 1}{\lambda_{m,n} + \lambda_{m,n}^*} = \zeta^2 \frac{e^{2\text{Re}(\lambda_{m,n})t} - 1}{2 \text{Re}(\lambda_{m,n})} \quad (17)$$

$$m, n = 0, \pm 1, \dots, \pm \infty; \quad m^2 + n^2 \neq 0$$

where $\text{Re}(\lambda_{m,n})$ denotes the real part of $\lambda_{m,n}$. For $z_{0,0}(t)$, it follows from eq 16 with $\lambda_{0,0} = 0$ that

$$\langle z_{0,0}(t) \rangle = t \pi c$$

$$\langle z_{0,0}^2(t) \rangle = \zeta^2 t + t^2 \pi^2 c^2 \quad (18)$$

It can be seen in eq 17 that the statistical moments of each stochastic ODE state depend only on the real part of the corresponding eigenvalue, and therefore, to determine the imaginary part of the eigenvalue we need to construct an extra equation. We note that $\lambda_{m,n}$ would be a complex number if the linear operator A is not self-adjoint, for example, when odd-partial-derivatives are present in the stochastic PDE (see eq 10).

Therefore, we rewrite eq 14 by separating the real part and the imaginary part of $z_{m,n}(t)$ as follows with initial condition $z_{m,n,0} = 0$:

$$z_{m,n}(t) = \frac{1}{2} \int_0^t [e^{\lambda_{m,n}(t-\mu)} + e^{\lambda_{m,n}^*(t-\mu)}] \xi_{m,n}(\mu) d\mu + \frac{1}{2} \int_0^t [e^{\lambda_{m,n}(t-\mu)} - e^{\lambda_{m,n}^*(t-\mu)}] \xi_{m,n}(\mu) d\mu \quad (19)$$

$$m, n = 0, \pm 1, \dots, \pm \infty; \quad m^2 + n^2 \neq 0$$

Accordingly, the real part of $z_{m,n}(t)$ can be expressed as follows:

$$\text{Re}[z_{m,n}(t)] = \frac{1}{2} \int_0^t [e^{\lambda_{m,n}(t-\mu)} + e^{\lambda_{m,n}^*(t-\mu)}] \xi_{m,n}(\mu) d\mu \quad (20)$$

$$m, n = 0, \pm 1, \dots, \pm \infty; \quad m^2 + n^2 \neq 0$$

where $\text{Re}[z_{m,n}(t)]$ denotes the real part of $z_{m,n}(t)$. By using result 1, we have

$$\langle \text{Re}[z_{m,n}(t)] \rangle = 0$$

$$\langle \text{Re}[z_{m,n}(t)]^2 \rangle$$

$$= \zeta^2 \left[\frac{\lambda_{m,n}^* e^{2\lambda_{m,n}t} + \lambda_{m,n} e^{2\lambda_{m,n}^*t} - (\lambda_{m,n} + \lambda_{m,n}^*)}{8 \lambda_{m,n} \lambda_{m,n}^*} + \frac{e^{(\lambda_{m,n} + \lambda_{m,n}^*)t} - 1}{2(\lambda_{m,n} + \lambda_{m,n}^*)} \right]$$

$$= \zeta^2 \left\{ \frac{\text{Re}(\lambda_{m,n}) e^{2\text{Re}(\lambda_{m,n})t} \cos(2 \text{Im}(\lambda_{m,n})t)}{4[\text{Re}(\lambda_{m,n})^2 + \text{Im}(\lambda_{m,n})^2]} + \frac{\text{Im}(\lambda_{m,n}) e^{2\text{Re}(\lambda_{m,n})t} \sin(2 \text{Im}(\lambda_{m,n})t)}{4[\text{Re}(\lambda_{m,n})^2 + \text{Im}(\lambda_{m,n})^2]} - \frac{\text{Re}(\lambda_{m,n})}{4[\text{Re}(\lambda_{m,n})^2 + \text{Im}(\lambda_{m,n})^2]} + \frac{e^{2\text{Re}(\lambda_{m,n})t} - 1}{4 \text{Re}(\lambda_{m,n})} \right\}$$

$$m, n = 0, \pm 1, \dots, \pm \infty; \quad m^2 + n^2 \neq 0 \quad (21)$$

where $\text{Im}(\lambda_{m,n})$ denotes the imaginary part of $\lambda_{m,n}$. Thus,

we can use eq 17 to first determine the real part of the eigenvalue and then use eq 21 to determine its imaginary part. We note that we can determine both parts of the eigenvalue using only eq 21; however, in that case, the nonlinear least-squares problem involved in the eigenvalue determination would be much more difficult to solve.

Remark 3. Equations 17, 18, and 21 show the analytical relation that relates the linear operator and the Gaussian noise in eq 4 to the statistical moments of the states of eq 12 which can be obtained through multiple experimental measurements or first-principle simulations and, therefore, reveal a viable path to systematically construct a linear stochastic PDE of the form of eq 4 that describes the dynamics of a microscopic process directly from experimental or simulation data.

3. Model Construction

Following the procedure we proposed in our previous work,²³ we construct a linear stochastic PDE for the deposition process described in section 2.1. The procedure includes the following steps: First, we design a set of simulation experiments that cover the complete range of process operation; second, we run multiple simulations for each simulation experiment to obtain the trajectories of the first and second statistical moments of the states (i.e., Fourier coefficients) computed from the surface snapshots; third, we compute the eigenvalues of the linear operator and covariance of the Gaussian noise based on the trajectories of the statistical moments of the states for each simulation experiment and determine the model parameters of the stochastic PDE (i.e., the prederivative coefficients and the order of the stochastic PDE); finally, we investigate the dependence of the model parameters of the stochastic PDE on the process parameters and determine the least-squares-optimal form of the stochastic PDE model with model parameters expressed as functions of the process parameters.

Remark 4. We note that all the simulation experiments are executed using simulation lattices whose sizes are large enough to capture the dynamics of the surface evolution during the thin film growth, and we run additional simulation experiments using larger lattices to ensure our results. As we have mentioned in ref 23, the experimental measurements obtained from the actual physical process can also be used for model construction, as long as the measurement has enough resolution to capture the surface evolution dynamics. Furthermore, since the same dynamics can be present at both large and small length scale, the resolution of the constructed model could be even better than the experimental measurements. In general, the use of a finite lattice size simulation and limited resolution measurements does not affect the accuracy of the constructed model, provided that the surface evolution dynamics are retained in the simulation/experimental data.

3.1. Eigenvalues and Covariance. The eigenvalues and the covariance of the systems of ODEs which correspond to the deposition processes with different W and T values are identified based on the trajectories of the statistical moments. In the previous section we have shown that for a deposition process with a flat initial surface, the trajectory of the second statistical moment of the ODE state $\langle z_{m,n}(t)z_{m,n}^*(t) \rangle$ can be predicted by eq

17; therefore, we can fit ζ^2 and $\text{Re}(\lambda_{m,n})$ in eq 17 for the profile of $\langle z_{m,n}(t)z_{m,n}^*(t) \rangle$. Similarly, $\text{Im}(\lambda_{m,n})$ can be determined based on the trajectory of $\langle \text{Re}[z_{m,n}(t)]^2 \rangle$ and eq 21.

To obtain the profile of $\langle z_{m,n}(t)z_{m,n}^*(t) \rangle$ and $\langle \text{Re}[z_{m,n}(t)]^2 \rangle$, we need to generate snapshots of the thin film surface during each deposition simulation and compute the values of $z_{m,n}(t)$. Since the lattice consists of discrete sites, we let $h(k_x L, k_y L, t)$ be the height profile of the surface at time t with lattice constant L (k_x and k_y denote the coordinates of a specific surface site) and compute $z_{m,n}(t)$ as follows:

$$\begin{aligned} z_{m,n}(t) &= \int_0^\pi \int_0^\pi h(x, y, t) \phi_{m,n}^*(x, y) dx dy \\ &= \sum_{k_x, k_y=0}^{k_{\max}} h(k_x L, k_y L, t) \int_{k_x L}^{(k_x+1)L} \int_{k_y L}^{(k_y+1)L} \phi_{m,n}^*(x, y) \\ &\quad dx dy \quad (22) \end{aligned}$$

where $k_{\max} L = \pi$ (i.e., the lattice is mapped to the domain $[0, \pi]^2$). Substituting eq 10 into eq 22, we can derive the following expressions for $z_{m,n}(t)$, $z_{0,n}(t)$, $z_{m,0}(t)$, and $z_{0,0}(t)$:

$$\begin{aligned} z_{m,n}(t) &= \sum_{k_x, k_y=0}^{k_{\max}} \frac{h(k_x L, k_y L, t)}{-4\pi m n} e^{-I2m k_x L + I2n k_y L} (e^{-I2m L} - 1)(e^{-I2n L} - 1) \quad (23) \\ &\quad m, n = \pm 1, \dots, \pm\infty \end{aligned}$$

$$\begin{aligned} z_{0,n}(t) &= \sum_{k_x, k_y=0}^{k_{\max}} \frac{h(k_x L, k_y L, t) L e^{-I2k_x n L}}{-I2\pi n} (e^{-I2n L} - 1) \quad (24) \\ &\quad n = \pm 1, \dots, \pm\infty \end{aligned}$$

$$\begin{aligned} z_{m,0}(t) &= \sum_{k_x, k_y=0}^{k_{\max}} \frac{h(k_x L, k_y L, t) L e^{-I2k_x m L}}{-I2\pi m} (e^{-I2m L} - 1) \quad (25) \\ &\quad m = \pm 1, \dots, \pm\infty \end{aligned}$$

$$z_{0,0}(t) = \sum_{k_x, k_y=0}^{k_{\max}} \frac{h(k_x L, k_y L, t) L^2}{\pi} \quad (26)$$

For each simulation experiment, the profiles of $\langle z_{m,n}(t)z_{m,n}^*(t) \rangle$ and $\langle \text{Re}[z_{m,n}(t)]^2 \rangle$ are computed based on 100 simulation runs taking place with the same process parameters (further increase in the number of simulations led to identical results for the order and the parameters of the constructed stochastic PDE).

Figure 2 shows an eigenspectrum identified from a thin film deposition (we note that the identified eigenvalues are considered real since the imaginary part of the eigenvalues identified turned out to be very small). It can be seen that the identified spectrum is very close to the parabolic reference curve (appears as a line when the eigenvalue is plotted against $m^2 + n^2$). Based on eq 10, this implies that a second-order stochastic PDE system of the following form would be able to describe the evolution of the surface height of this deposition process:

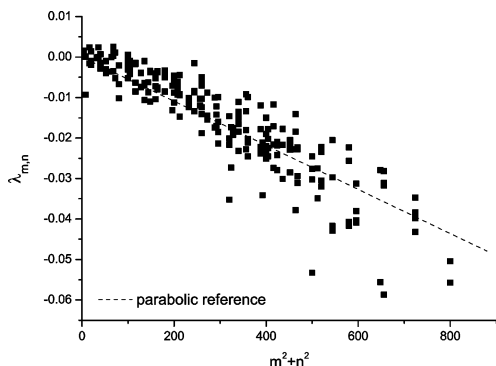


Figure 2. Eigenvalue spectrum of the infinite stochastic ODE systems identified from the kMC simulation of the deposition process with $W = 0.5$ 1/s, $T = 650$ K, and $k_{\max} = 100$.

$$\frac{\partial h}{\partial t} = c + c_2 \nabla^2 h + \xi(x, y, t)$$

$$\nabla h(0, y, t) = \nabla h(\pi, y, t), \quad h(0, y, t) = h(\pi, y, t),$$

$$\nabla h(x, 0, t) = \nabla h(x, \pi, t), \quad h(x, 0, t) = h(x, \pi, t),$$

$$h(x, y, 0) = h_0(x, y) \quad (27)$$

in which c , c_2 , and the covariance of the Gaussian noise ξ , ζ , all depend on the microscopic processes and operating conditions.

Remark 5. We note that it is necessary to rescale $m^2 + n^2$ with the square of the corresponding lattice size, to carry out a meaningful comparison among eigenspectrums identified from simulations using lattices of different size, and for the same reason, the covariance values should be scaled with the inverse of the square of the lattice size, $1/k_{\max}^2$ (see ref 23 for a detailed discussion).

3.2. Dependence on the Process Parameters. We proceed now with the derivation of the parameters of the stochastic PDE of eq 27. c , c_2 , and ζ^2 are evaluated for assorted deposition conditions, and the lattice size of 100×100 (i.e., $k_{\max} = 100$) is used for all the simulation runs in our study.

Model parameter c is determined using eq 18 based on the trajectory of $\langle z_{0,0}(t) \rangle$. Since $z_{0,0}(t)$ is, in fact, proportional to the average height (see eq 26, i.e., the thickness of the film), c should equal the adsorption rate W when there is no desorption of surface molecules (see the process studied in ref 23 for example). However, desorption of surface molecules is significant in the deposition process studied in this work, and thus, the actual value of c should be smaller than W . Therefore, to derive the expression for c , we plot the relative difference of c and W (i.e., $(W - c)/W$) against W and T , and the result is shown in Figure 3. It can be seen in Figure 3 that $\ln[(W - c)/W]$ has a quasi-linear relationship with both T and $\ln W$, and thus, the following expression can be obtained for c as a function of T and W through least-squares fitting:

$$c(W, T) = W \left(1 - \frac{k_w}{W^{a_w} e^{-k_B T/E_w}} \right) \quad (28)$$

where $k_w = 3.3829 \times 10^{-12}$, $a_w = 0.6042$, and $E_w = 2.7 \times 10^{-3}$ eV.

The value of c_2 is determined by least-squares fitting of eq 10 and the eigenspectrum identified from the simulation. Figure 4 shows the profile of c_2 as a function of T and W . It can be seen that $\ln c_2$ has a quasi-linear

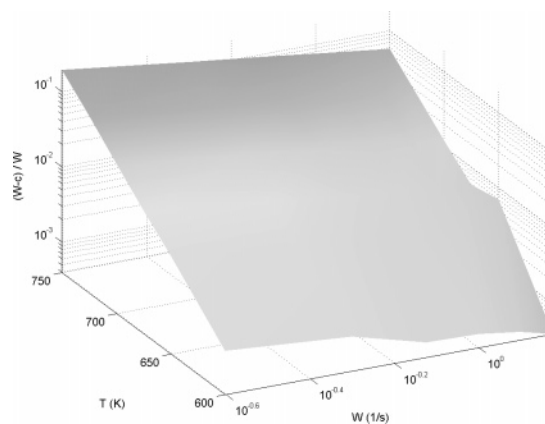


Figure 3. Profile of $(W - c)/W$ as a function of substrate temperature T and adsorption rate W .

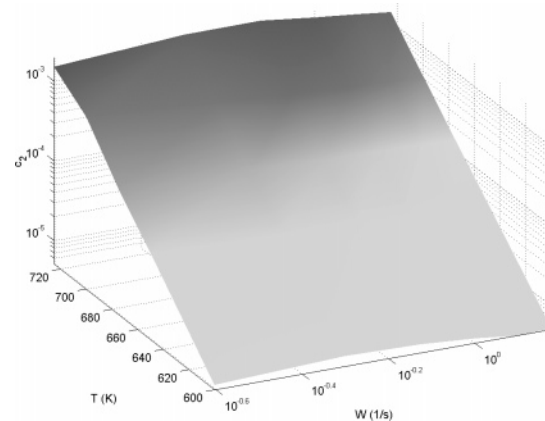


Figure 4. Profile of c_2 as a function of substrate temperature T and adsorption rate W .

relationship with both T and $\ln W$, and thus, the following expression can be obtained for c_2 as a function of T and W through least-squares fitting:

$$c_2(W, T) = \frac{k_{c0}}{W^{a_c} e^{-k_B T/E_c}} = \frac{k_c}{k_{\max}^2 W^{a_c} e^{-k_B T/E_c}} \quad (29)$$

where $k_c = 1.0274 \times 10^{-13}$, $a_c = 0.1669$, and $E_c = 1.9 \times 10^{-3}$ eV.

The value of ζ^2 is obtained by averaging the ζ^2 values determined using eq 17 based on the trajectories of the second statistical moments of the states. However, derivation of the expression of $\zeta^2(T, W)$ is not as straightforward as the ones for c and c_2 . Figure 5 shows the profile of the normalized ζ^2 value, $\zeta^2/(\pi/k_{\max})^2$, as a function of T for different W . It can be noticed that $\zeta^2/(\pi/k_{\max})^2$ grows exponentially with W , and therefore we may assume $\zeta^2/(\pi/k_{\max})^2 = 1 + e^{a_{v0} + k_{v0}T}$. Values of a_{v0} and k_{v0} are determined by least-squares fitting for different W , and results suggest that a_{v0} and k_{v0} are linear functions of W . Thus, the following expression is obtained for ζ^2 as a function of T and W :

$$\begin{aligned} \zeta^2(W, T) &= \frac{\pi^2}{k_{\max}^2} W [1 + e^{-a_v - k_v W + (a_t + k_t W) T}] \\ &= \frac{\pi^2}{k_{\max}^2} W \left[1 + \frac{e^{(a_t + k_t W) T}}{e^{a_v + k_v W}} \right] \end{aligned} \quad (30)$$

where $a_v = 15.55493$, $k_v = 20.64504$, $a_t = 0.02332$, and $k_t = 0.0261$.

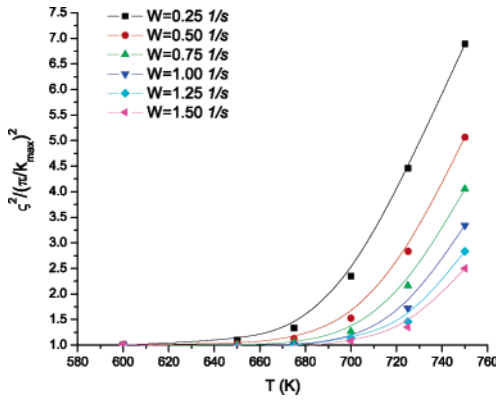


Figure 5. Profile of $\zeta^2/(\pi/k_{\max})^2$ as a function of substrate temperature T for different adsorption rates.

Therefore, the linear stochastic PDE model identified for the deposition process is as follows:

$$\begin{aligned} \frac{\partial h}{\partial t} &= W \left(1 - \frac{k_w}{W^{a_w} e^{-k_B T/E_w}} \right) + \left(\frac{k_c}{k_{\max}^2 W^{a_c} e^{-k_B T/E_c}} \right) \nabla^2 h + \xi(x, y, t) \\ \nabla h(0, y, t) &= \nabla h(\pi, y, t), \quad h(0, y, t) = h(\pi, y, t), \\ \nabla h(x, 0, t) &= \nabla h(x, \pi, t), \quad h(x, 0, t) = h(x, \pi, t), \\ h(x, y, 0) &= h_0(x, y) \end{aligned} \quad (31)$$

where

$$\begin{aligned} \langle \xi(x, y, t) \xi^*(x', y', t') \rangle &= \\ &= \frac{\pi^2}{k_{\max}^2} W \left[1 + \frac{e^{(a_i + k_i) W T}}{e^{a_i + k_i W}} \right] \delta(x - x') \delta(y - y') \delta(t - t') \end{aligned}$$

3.3. Validation of Stochastic PDE Model. We now proceed with the validation of the stochastic PDE model of the thin film deposition process (eq 31). Validation experiments are conducted for a number of deposition conditions which have not been used for the model construction. We generate surface profiles using both the stochastic PDE model and the kinetic Monte Carlo simulation. Figure 6 shows the surface profile at the end of a deposition with substrate temperature $T = 610$ K, adsorption rate $W = 0.5$ 1/s, deposition duration of 200 s, and $k_{\max} = 100$; Figure 7 shows the surface profile at the end of a deposition with substrate temperature $T = 710$ K, adsorption rate $W = 0.5$ 1/s, deposition duration of 200 s, and lattice size $k_{\max} = 100$; we can see that at both low and high substrate temperatures, the linear stochastic PDE model constructed for the deposition process is very consistent with the kinetic Monte Carlo simulation in terms of film thickness and surface morphology (such as surface island size distribution and aggregation). The only observable difference between the two surfaces is that the one generated by kMC simulation has finer structural details than the one generated by stochastic PDE simulation. Such difference is caused, on one hand, by the fact that the surface height profile in the stochastic PDE model is a continuous approximation of the discrete lattice and, on the other hand, by the error that occurs in the stochastic PDE simulation in which a finite-dimensional stochastic ODE approximation of the original stochastic PDE is used (this error can be reduced by increasing the order of the finite-dimensional approximation).

In addition, we generate expected surface roughness profiles using both the stochastic PDE model and the kinetic Monte Carlo simulation (average of 100 runs) for the deposition process. For simplicity, the surface roughness is evaluated in a root-mean-square fashion as follows:

$$r(t) = \sqrt{\frac{1}{\pi^2} \int_0^\pi \int_0^\pi [h(x, y, t) - \bar{h}(t)]^2 dx dy} \quad (32)$$

where $\bar{h}(t) = 1/\pi^2 \int_0^\pi \int_0^\pi h(x, y, t) dx dy$ is the average surface height. We note that for more detailed descriptions of the surface morphology, the surface can be examined using the height–height correlation function²⁷ and the interface width function.²⁸

To calculate the expected surface roughness using the stochastic PDE model, we first expressed the surface roughness in terms of the ODE states. According to eq 22, we have $\bar{h}(t) = z_{0,0}(t)\phi_{0,0}$. Therefore, $r(t)$ can be rewritten in terms of $z_{m,n}$ as follows:

$$\begin{aligned} r(t) &= \sqrt{\frac{1}{\pi^2} \int_0^\pi \int_0^\pi [h(x, y, t) - \bar{h}(t)][h(x, y, t) - \bar{h}(t)]^* dx dy} \\ &= \sqrt{\frac{1}{\pi^2} \int_0^\pi \int_0^\pi \sum_{m,n=-\infty, m^2+n^2 \neq 0}^{\infty} z_{m,n}(t) \phi_{m,n}(x, y) \phi_{m,n}^*(x, y) z_{m,n}^*(t) dx dy} \\ &= \sqrt{\frac{1}{\pi^2} \sum_{m,n=-\infty, m^2+n^2 \neq 0}^{\infty} z_{m,n}(t) z_{m,n}^*(t)} \end{aligned} \quad (33)$$

and the expected roughness can be computed as follows:

$$\langle r(t) \rangle = \sqrt{\frac{1}{\pi^2} \sum_{m,n=-\infty, m^2+n^2 \neq 0}^{\infty} \langle z_{m,n}(t) z_{m,n}^*(t) \rangle} \quad (34)$$

Substituting eq 16 and $\lambda_n = -4c_2(m^2 + n^2)$ into eq 34, we obtain the following expression of the trajectory of $\langle r(t) \rangle$ in terms of the parameters of the stochastic PDE model:

$$\langle r(t) \rangle = \sqrt{\frac{1}{\pi^2} \sum_{m,n=-\infty, m^2+n^2 \neq 0}^{\infty} \left[\frac{e^{-8c_2(m^2+n^2)t} - 1}{-8c_2(m^2 + n^2)} + e^{-8c_2(m^2+n^2)t} z_{m,n,0} z_{m,n,0}^* \right]} \quad (35)$$

Figure 8 shows the expected roughness profile of a deposition with substrate temperature $T = 610$ K and adsorption rate $W = 0.5$ 1/s; Figure 9 shows the roughness profile of a deposition with substrate temperature $T = 710$ K and adsorption rate $W = 0.5$ 1/s; we can see that the roughness profiles generated by the linear stochastic PDE model are very close to the profiles generated by the kinetic Monte Carlo simulation, for both low and high substrate temperatures.

Furthermore, we also generate expected thin film thickness profiles using both the stochastic PDE model and the kinetic Monte Carlo simulation (average of 100 runs) for the deposition process (shown in Figure 10).

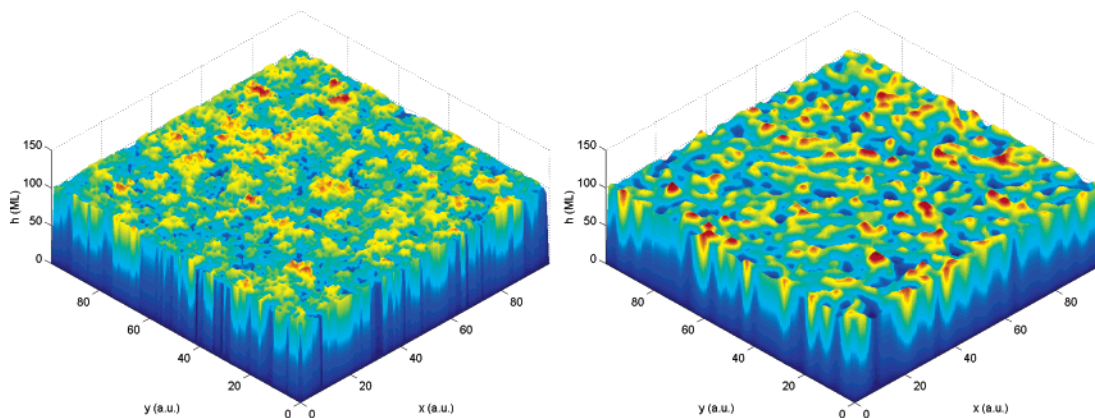


Figure 6. Final thin film surface profiles generated by kMC simulation (left, $k_{\max} = 100$) and stochastic PDE model (right, 20×20 states) for a 200 s deposition with substrate temperature $T = 610$ K and adsorption rate $W = 0.5$ 1/s.

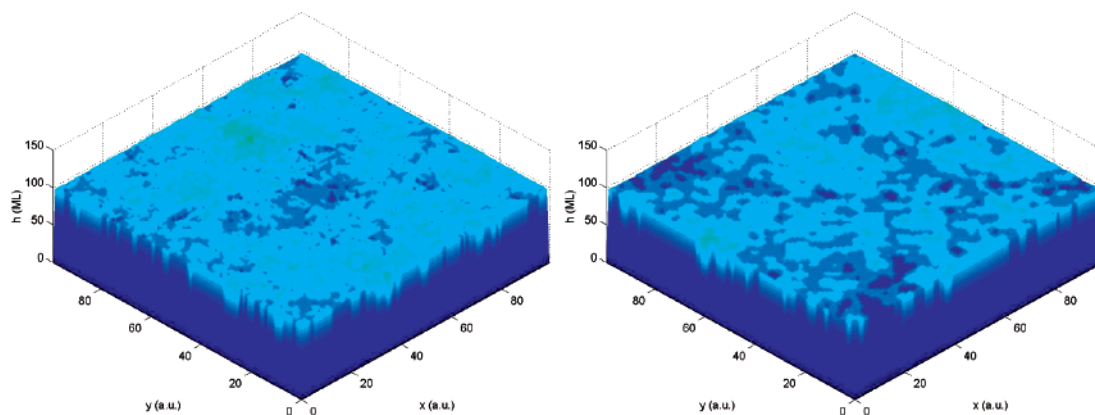


Figure 7. Final thin film surface profiles generated by kMC simulation (left, $k_{\max} = 100$) and stochastic PDE model (right, 20×20 states) for a 200 s deposition with substrate temperature $T = 710$ K and adsorption rate $W = 0.5$ 1/s.

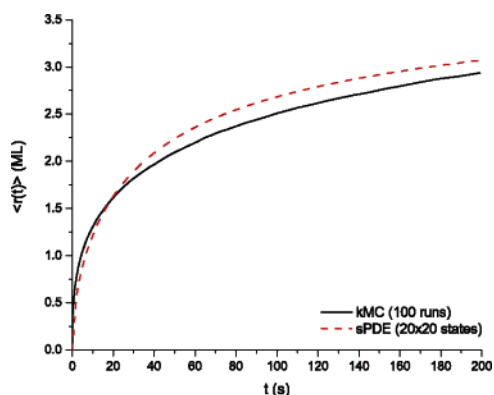


Figure 8. Expected surface roughness profiles generated by kMC simulation ($k_{\max} = 100$) and stochastic PDE model for a 200 s deposition with substrate temperature $T = 610$ K and adsorption rate $W = 0.5$ 1/s.

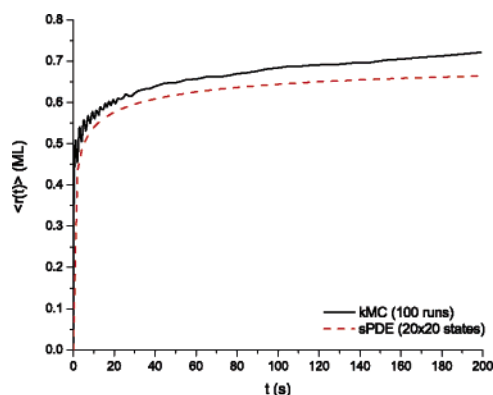


Figure 9. Expected surface roughness profiles generated by kMC simulation ($k_{\max} = 100$) and stochastic PDE model for a 200 s deposition with substrate temperature $T = 710$ K and adsorption rate $W = 0.5$ 1/s.

We can see that the thickness profiles generated by the linear stochastic PDE model are also very close to the profiles generated by the kinetic Monte Carlo simulation, for both low and high substrate temperatures.

4. Feedback Control

In this section, we design a multivariable state feedback controller based on the stochastic PDE model of eq 31 to control the thin film thickness and surface roughness for the deposition process. The difficulty of obtaining in situ surface measurements in real time had been one of the obstacles for implementing feedback

control systems on thin film processes. Recently, researchers made possible the use of some of the intrusive scanning probe based techniques such as scanning tunneling microscopy (STM),²⁹ secondary electron microscopy (SEM),³⁰ and atomic force microscopy (AFM)³¹ in situ, to observe in real time the growth of the thin film. In ref 32, it was reported that a nonintrusive grazing incidence small-angle X-ray scattering (GISAXS) method was successfully used to monitor the thin film growth in situ in real time; the method was capable of sampling large surface areas with sampling frequency up to 10 Hz and a subnanometer resolution. Such advancements in surface metrology indeed create the

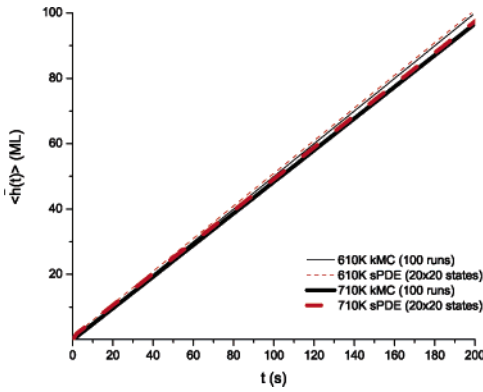


Figure 10. Expected thin film thickness profiles generated by kMC simulation ($k_{\max} = 100$) and stochastic PDE model for (1) a 200 s deposition with substrate temperature $T = 610$ K and adsorption rate $W = 0.5$ 1/s (thin lines) and (2) a 200 s deposition with substrate temperature $T = 710$ K and adsorption rate $W = 0.5$ 1/s (thick lines).

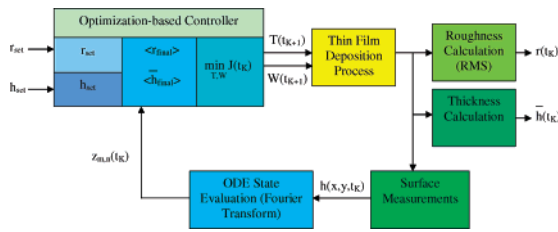


Figure 11. Block diagram of the closed-loop system.

possibility for implementing feedback control systems which rely on real-time surface state measurements.

Since the thin film deposition is a batch process, the control objective is to control the final thin film thickness and surface roughness to the desired levels at the end of each deposition run. We use an optimization-based control problem formulation. The substrate temperature T and the adsorption rate W (W can be adjusted by varying reactor inlet gas flow rate, chamber pumping speed, etc.) are chosen to be the manipulated variables. Furthermore, since the process is stochastic in nature, the controlled variables are the expected values of the final thin film thickness $\langle \hat{h}(t_{\text{dep}}) \rangle$ and of the surface roughness $\langle \hat{r}(t_{\text{dep}}) \rangle$, where t_{dep} is the total deposition time.

Figure 11 shows the block diagram of the closed-loop system. The control system operates in a discrete time fashion; when the K th real-time surface profile measurement is obtained at time t_K (i.e., $t_K = Kt_s$, where t_s is the measurement interval as well as the control interval), the states of the infinite stochastic ODE system, $z_{m,n}(t_K)$, are computed. Then, a substrate temperature $T(t_{K+1})$ and an adsorption rate $W(t_{K+1})$ are computed based on states $z_{m,n}(t_K)$ and the stochastic PDE model, under the assumption that T and W are held at designated levels for the rest of the deposition. $T(t_{K+1})$ and $W(t_{K+1})$ are then applied to the deposition process at the next measurement time t_{K+1} .

4.1. Predictive Control Design. To design a model-based predictive controller, we first derive the analytical expression for the trajectory of $\langle \hat{h}(t) \rangle$ and $\langle \hat{r}(t) \rangle$. Due to the fact that the current deposition parameters ($T(t_K)$ and $W(t_K)$) would be used during the current control cycle before the new levels ($T(t_{K+1})$ and $W(t_{K+1})$) are applied, the estimate of the film thickness (i.e., the estimate of $\langle z_{0,0}(t_{\text{dep}}) \rangle$) and the estimate of the final surface roughness cannot be computed directly using

eqs 18 and 35 ($\lambda_{m,n}$ and ζ^2 are no longer constant due to the change of W and T). Therefore, we first need to derive the expressions of $z_{0,0}(t_{\text{dep}})$ and $z_{m,n}(t_{\text{dep}})$ ($m^2 + n^2 \neq 0$) for this case. We consider that at time t_{K+1} , the deposition parameters are changed from $W(t_K)$ and $T(t_K)$ to $W(t_{K+1})$ and $T(t_{K+1})$, respectively. Following from eq 14, we have

$$z_{0,0}(t) = z_{0,0}(t_0) + c_{0,0}^z(t - t_0) + \int_{t_0}^t \xi_{0,0}(\mu) d\mu$$

$$z_{m,n}(t) = e^{\lambda_{m,n}(t-t_0)} z_{m,n}(t_0) + \int_{t_0}^t e^{\lambda_{m,n}(t-\mu)} \xi_{m,n}(\mu) d\mu \quad (36)$$

$$m, n = 0, \pm 1, \dots, \pm \infty; \quad m^2 + n^2 \neq 0$$

Hence, by calculating the intermediate values $z_{0,0}(t_{K+1})$ and $z_{m,n}(t_{K+1})$ ($m^2 + n^2 \neq 0$) using $z_{0,0}(t_K)$ and $z_{m,n}(t_K)$, respectively, the expressions of $z_{0,0}(t_{\text{dep}})$ and $z_{m,n}(t_{\text{dep}})$ can be derived as follows:

$$z_{0,0}(t_{\text{dep}}) = z_{0,0}(t_K) + c_{0,0}^z(t_K)t_c + c_{0,0}^z(t_{K+1})(t_{\text{dep}} - t_{K+1}) + \int_{t_K}^{t_{K+1}} \xi_{0,0}(\mu) d\mu + \int_{t_{K+1}}^{t_{\text{dep}}} \xi_{0,0}(\mu) d\mu$$

$$z_{m,n}(t) = e^{\lambda_{m,n}(t_K)t_c + \lambda_{m,n}(t_{K+1})(t_{\text{dep}} - t_{K+1})} z_{m,n}(t_K) + e^{\lambda_{m,n}(t_{K+1})t_c} \int_{t_K}^{t_{K+1}} e^{\lambda_{m,n}(t_K)(t_{K+1} - \mu)} \xi_{m,n}(\mu) d\mu + \int_{t_{K+1}}^{t_{\text{dep}}} e^{\lambda_{m,n}(t_{K+1})(t_{\text{dep}} - \mu)} \xi_{m,n}(\mu) d\mu \quad (37)$$

$$m, n = 0, \pm 1, \dots, \pm \infty; \quad m^2 + n^2 \neq 0$$

Using result 1 and substituting $c_{0,0}^z = \pi c$ and $\lambda_{m,n} = -4(m^2 + n^2)c_2$ (eq 10), the above equations can be simplified as follows:

$$z_{0,0}(t_{\text{dep}}) = z_{0,0}(t_K) + \pi c(t_K)t_c + \pi c(t_{K+1})(t_{\text{dep}} - t_{K+1}) + \bar{\theta}_{0,0}(t_K) + \hat{\theta}_{0,0}(t_{K+1})$$

$$z_{m,n}(t) = e^{-4(m^2+n^2)\{c_2(t_K)t_c + c_2(t_{K+1})(t_{\text{dep}} - t_{K+1})\}} z_{m,n}(t_K) + \bar{\theta}_{m,n}(t_K) + \hat{\theta}_{m,n}(t_{K+1})$$

$$m, n = 0, \pm 1, \dots, \pm \infty; \quad m^2 + n^2 \neq 0 \quad (38)$$

where $\bar{\theta}_{0,0}(t_K)$, $\hat{\theta}_{0,0}(t_{K+1})$, $\bar{\theta}_{m,n}(t_K)$, and $\hat{\theta}_{m,n}(t_{K+1})$ ($m^2 + n^2 \neq 0$) are independent Gaussian random numbers with zero mean, and their covariances can be expressed as follows:

$$\langle \bar{\theta}_{0,0}(t_K) \bar{\theta}_{0,0}^*(t_K) \rangle = \zeta^2(t_K)t_c$$

$$\langle \hat{\theta}_{0,0}(t_{K+1}) \hat{\theta}_{0,0}^*(t_{K+1}) \rangle = \zeta^2(t_{K+1})(t_{\text{dep}} - t_{K+1})$$

$$\langle \bar{\theta}_{m,n}(t_K) \bar{\theta}_{m,n}^*(t_K) \rangle = e^{-8(m^2+n^2)c_2(t_{K+1})t_c} \zeta^2(t_K) \frac{e^{-8(m^2+n^2)c_2(t_K)t_c} - 1}{-8(m^2 + n^2)c_2(t_K)}$$

$$\langle \hat{\theta}_{m,n}(t_{K+1}) \hat{\theta}_{m,n}^*(t_{K+1}) \rangle = \zeta^2(t_{K+1}) \frac{e^{-8(m^2+n^2)c_2(t_{K+1})(t_{\text{dep}} - t_{K+1})} - 1}{-8(m^2 + n^2)c_2(t_{K+1})} \quad (39)$$

$$m, n = 0, \pm 1, \dots, \pm \infty; \quad m^2 + n^2 \neq 0$$

Therefore, the quantities that directly relate to thickness and roughness estimations, $\langle z_{0,0}(t_{\text{dep}}) \rangle$, $\langle z_{m,n}(t_{\text{dep}}) \rangle$,

and $\langle z_{m,n}(t_{\text{dep}})z_{m,n}^*(t_{\text{dep}}) \rangle$, can be derived as follows:

$$\begin{aligned} \langle z_{0,0}(t_{\text{dep}}) \rangle &= z_{0,0}(t_K) + \pi c(t_K)t_c + \\ &\quad \pi c(t_{K+1})(t_{\text{dep}} - t_{K+1}) \\ \langle z_{m,n}(t_{\text{dep}}) \rangle &= e^{-4(m^2+n^2)[c_2(t_K)t_c + c_2(t_{K+1})(t_{\text{dep}} - t_{K+1})]} z_{m,n}(t_K) \\ \langle z_{m,n}(t_{\text{dep}})z_{m,n}^*(t_{\text{dep}}) \rangle &= \langle z_{m,n}(t_{\text{dep}}) \rangle \langle z_{m,n}(t_{\text{dep}}) \rangle^* + \\ &\quad \langle \hat{\theta}_{m,n}(t_K)\hat{\theta}_{m,n}^*(t_K) \rangle + \langle \hat{\theta}_{m,n}(t_{K+1})\hat{\theta}_{m,n}^*(t_{K+1}) \rangle \quad (40) \\ m, n &= 0, \pm 1, \dots, \pm \infty; \quad m^2 + n^2 \neq 0 \end{aligned}$$

Accordingly, the expected final film thickness can be expressed as follows:

$$\langle \bar{h}_{\text{final}}(t_K) \rangle = \frac{\langle z_{0,0}(t_{\text{dep}}) \rangle}{\pi} = \frac{z_{0,0}(t_K)}{\pi} + c(t_K)t_c + c(t_{K+1})(t_{\text{dep}} - t_{K+1}) \quad (41)$$

Also, by substituting eq 40 into eq 34, the expected final surface roughness can be derived as follows:

$$\begin{aligned} \langle r_{\text{final}}(t_K) \rangle^2 &= \frac{1}{\pi^2} \sum_{m,n=-\infty; m^2+n^2 \neq 0}^{\infty} \langle z_{m,n}(t_{\text{dep}})z_{m,n}^*(t_{\text{dep}}) \rangle \\ &= \frac{1}{\pi^2} \sum_{m,n=-\infty; m^2+n^2 \neq 0}^{\infty} [\langle z_{m,n}(t_{\text{dep}}) \rangle \langle z_{m,n}(t_{\text{dep}}) \rangle^* + \\ &\quad \langle \hat{\theta}_{m,n}(t_K)\hat{\theta}_{m,n}^*(t_K) \rangle + \langle \hat{\theta}_{m,n}(t_{K+1})\hat{\theta}_{m,n}^*(t_{K+1}) \rangle] \\ &= \frac{1}{\pi^2} \sum_{m,n=-\infty; m^2+n^2 \neq 0}^{\infty} \left\{ z_{m,n}(t_K)z_{m,n}^*(t_K) \right. \\ &\quad \left. e^{-8(m^2+n^2)[c_2(t_K)t_c + c_2(t_{K+1})(t_{\text{dep}} - t_{K+1})]} + \right. \\ &\quad \left. e^{-8(m^2+n^2)c_2(t_{K+1})t_c} \zeta^2(t_K) \frac{e^{-8(m^2+n^2)c_2(t_K)t_c} - 1}{-8(m^2+n^2)c_2(t_K)} + \right. \\ &\quad \left. \zeta^2(t_{K+1}) \frac{e^{-8(m^2+n^2)c_2(t_{K+1})(t_{\text{dep}} - t_{K+1})} - 1}{-8(m^2+n^2)c_2(t_{K+1})} \right\} \quad (42) \end{aligned}$$

Since the computation of the above equation involves infinite summations, it cannot be calculated directly in practice. A finite dimensional approximation, which only uses the first ($\pm N$ th, $\pm N$ th) states, is used for the computation and is of the following form:

$$\begin{aligned} \langle r_{\text{final}}(t_K) \rangle^2 &= \frac{1}{\pi^2} \sum_{m,n=-N; m^2+n^2 \neq 0}^N \left\{ z_{m,n}(t_K)z_{m,n}^*(t_K) \right. \\ &\quad \left. e^{-8(m^2+n^2)[c_2(t_K)t_c + c_2(t_{K+1})(t_{\text{dep}} - t_{K+1})]} + \right. \\ &\quad \left. e^{-8(m^2+n^2)c_2(t_{K+1})t_c} \zeta^2(t_K) \frac{e^{-8(m^2+n^2)c_2(t_K)t_c} - 1}{-8(m^2+n^2)c_2(t_K)} + \right. \\ &\quad \left. \zeta^2(t_{K+1}) \frac{e^{-8(m^2+n^2)c_2(t_{K+1})(t_{\text{dep}} - t_{K+1})} - 1}{-8(m^2+n^2)c_2(t_{K+1})} \right\} \quad (43) \end{aligned}$$

Here we note that this finite dimensional approximation can be improved by utilizing an upper bound for the residue of the infinite summation derived following the method we proposed in our previous work (see ref 23 for detailed discussions on the convergence property

of the infinite series and the determination of N for a desired approximation precision); however, such improvement is not adopted in this work for simplicity. Moreover, instead of direct truncation of the system of infinite dimensional stochastic ODEs, more advanced reduction techniques can be used, especially when the stochastic PDE model is nonlinear (see refs 33 and 34 for results on nonlinear model reduction of parabolic PDEs). Therefore, the values of $T(t_{K+1})$ and $W(t_{K+1})$ are determined at each sampling time interval by solving, in the control time interval, the following optimization problem:

$$\min_{W(t_{K+1}), T(t_{K+1})} J(t_K) = q_h(h_{\text{set}} - \langle \bar{h}_{\text{final}}(t_K) \rangle)^2 + q_r(r_{\text{set}}^2 - \langle r_{\text{final}}(t_K) \rangle^2)^2 \quad (44)$$

subject to

$$\langle \bar{h}_{\text{final}}(t_K) \rangle = \frac{z_{0,0}(t_K)}{\pi} + c(t_K)t_c + c(t_{K+1})(t_{\text{dep}} - t_{K+1}) \quad (45)$$

$$\begin{aligned} \langle r_{\text{final}}(t_K) \rangle^2 &= \\ &= \frac{1}{\pi^2} \sum_{m,n=-N; m^2+n^2 \neq 0}^N \left\{ z_{m,n}(t_K)z_{m,n}^*(t_K) \right. \\ &\quad \left. e^{-8(m^2+n^2)[c_2(t_K)t_c + c_2(t_{K+1})(t_{\text{dep}} - t_{K+1})]} + \right. \\ &\quad \left. e^{-8(m^2+n^2)c_2(t_{K+1})t_c} \zeta^2(K) \frac{e^{-8(m^2+n^2)c_2(t_K)t_c} - 1}{-8(m^2+n^2)c_2(t_K)} + \right. \\ &\quad \left. \zeta^2(t_{K+1}) \frac{e^{-8(m^2+n^2)c_2(t_{K+1})(t_{\text{dep}} - t_{K+1})} - 1}{-8(m^2+n^2)c_2(t_{K+1})} \right\} \quad (46) \end{aligned}$$

$$c(t_{K+1}) = W(t_{K+1}) \left[1 - \frac{k_w}{W(t_{K+1})^{a_w} e^{-k_B T(t_{K+1})/E_w}} \right] \quad (47)$$

$$c_2(t_{K+1}) = \frac{k_c}{k_{\text{max}}^2 W(t_{K+1})^{a_c} e^{-k_B T(t_{K+1})/E_c}} \quad (48)$$

$$\zeta^2(t_{K+1}) = \frac{\pi^2}{k_{\text{max}}^2} W(t_{K+1}) \left\{ 1 + \frac{e^{[a_t + k_t W(t_{K+1})]T(t_{K+1})}}{e^{a_v + k_v W(t_{K+1})}} \right\} \quad (49)$$

$$c(t_{K+1}) \geq c_{\text{min}} \quad (50)$$

$$T_{\text{min}} \leq T(t_{K+1}) \leq T_{\text{max}} \quad (51)$$

$$W_{\text{min}} \leq W(t_{K+1}) \leq W_{\text{max}} \quad (52)$$

where q_h and q_r are the weights of the penalties on thickness and roughness, respectively; c_{min} is the minimum growth rate; T_{min} , T_{max} , W_{min} , and W_{max} are the lowest and highest substrate temperature and the lowest and highest adsorption rate, respectively. In this study, we use $q_h = 1/h_{\text{set}}^2$, $q_r = 1/r_{\text{set}}^2$, $c_{\text{min}} = 0.1 h_{\text{set}}/t_{\text{dep}}$, $T_{\text{min}} = 400 \text{ K}$, $T_{\text{max}} = 900 \text{ K}$, $W_{\text{min}} = 0.1 \text{ 1/s}$, and $W_{\text{max}} = 2.0 \text{ 1/s}$.

We note that J corresponds to the difference between the square of the desired final surface roughness r_{set} and the square of the estimated final surface roughness $\langle r_{\text{final}} \rangle$ computed based on the current states $z_{m,n}(t_K)$. We choose to minimize the difference of the squares of the

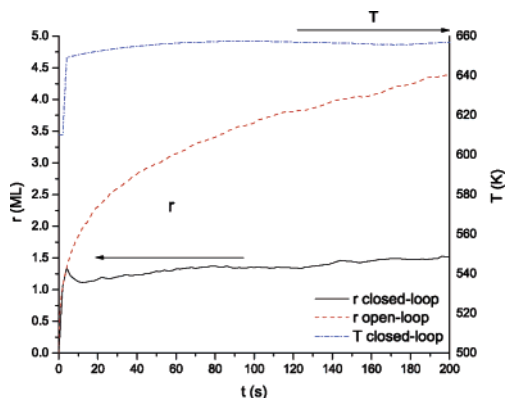


Figure 12. Surface roughness and substrate temperature profiles of a 200 s closed-loop deposition process with a thickness setpoint of 100 ML and a final roughness setpoint $r_{\text{set}} = 1.5$ ML; the initial deposition conditions are $T = 610$ K and $W = 1.0$ 1/s.

surface roughness, i.e., the mean square of the surface height, to simplify the calculation. The optimization problem is solved using a standard sequential quadratic programming (SQP) method described in ref 35.

Remark 6. Since eq 46 is a finite dimensional approximation of the predicted final surface roughness, to achieve a control precision ϵ , m should be chosen large enough for each optimization computation so that the approximation error is less than ϵ (see detailed discussion in ref 23).

Remark 7. Since the control action is computed using closed-form equations, the computation cost is proportional to the number of states used, $4N^2$, but independent of the optimization horizon $t_{\text{dep}} - t$; however, to evaluate the values of the $4N^2$ states, an additional computation time of the order of $4k_{\text{max}}^2N^2$ is needed for each surface measurement. Nevertheless, even for a lattice size that corresponds to the largest physical dimension of the sampling area that can be achieved by common surface measurement techniques (i.e., a few microns), such computation can still be completed within the control interval using currently available computing power. On the other hand, such task is almost impossible to achieve using a kMC code, whose computation cost is on the order of $k_{\text{max}}^4(t_{\text{dep}} - t)$ for merely a single run. Furthermore, we note that the evaluation of each state is independent of other states and, therefore, can be executed in parallel, while the kMC code, being a serial calculation, is unsuitable for parallel processing.

4.2. Closed-Loop Simulations. A kMC code using a lattice size of 100×100 is used to simulate the thin film deposition process, and t_c is set to be 1 s. The dimension of the finite dimensional approximation of the stochastic PDE used for optimization is $N = 10$.

Figure 12 shows the surface roughness and substrate temperature profiles of a closed-loop deposition process with initial substrate temperature $T = 610$ K and adsorption rate $W = 1.0$ 1/s (These initial values are picked such that, with process parameters fixed at these levels throughout the deposition, the final thickness and surface roughness of the deposited film are quite different from the desired values). Figure 13 shows the thin film thickness and surface adsorption rate profiles of this closed-loop deposition. The control objective is to control the thin film thickness to 100 ML and to drive the final surface roughness to 1.5 ML at the end of the 200 s deposition. It can be seen that both the film thickness and the final surface roughness are controlled

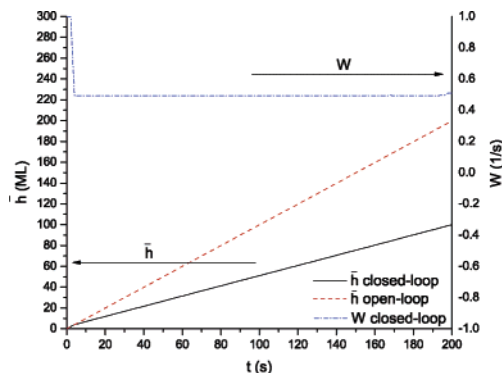


Figure 13. Thickness and surface adsorption rate profiles of a 200 s closed-loop deposition process with a thickness setpoint of 100 ML and a final roughness setpoint $r_{\text{set}} = 1.5$ ML; the initial deposition conditions are $T = 610$ K and $W = 1.0$ 1/s.

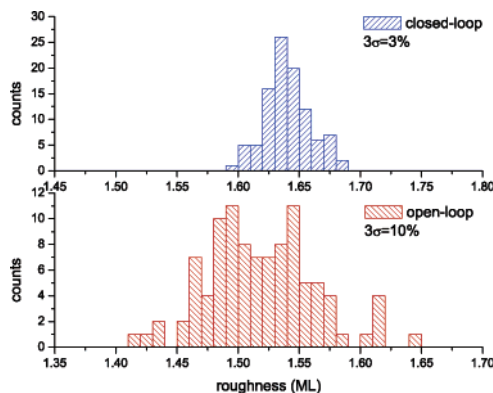


Figure 14. Histogram of final surface roughness of 100 closed-loop and 100 open-loop thin film depositions targeted at the same surface roughness level.

at the desired levels simultaneously while an open-loop deposition with the same initial deposition condition would lead to a 100% higher film thickness and a 100% higher final surface roughness as shown in Figure 12 and Figure 13.

Figure 14 shows the final surface roughness histogram of the thin films deposited using 100 different closed-loop depositions targeting a thin film thickness of 100 monolayers and a final surface roughness of 1.65 ML and 100 different open-loop depositions with fixed substrate temperature and surface adsorption rate. The average roughness of the thin films deposited by open-loop depositions is 1.52 ML, which is quite close to the average roughness of the thin films deposited by the closed-loop depositions (1.64 ML). However, the variance among the thin films from different open-loop deposition runs is over 300% higher than that of closed-loop depositions even though no process disturbance is considered in the simulations.

Such large variance among the films deposited by open-loop deposition can be attributed to the stochastic nature of the thin film growth process itself. Although optimal profiles of adsorption rate and substrate temperature, i.e., a well-prescribed process recipe, can be determined for the open-loop deposition, so that the average final thickness and surface roughness of the deposited films are very close to the desired levels, the stochasticity of the film growth cannot be effectively handled by the predetermined process recipes (implemented in an open-loop fashion) and, therefore, results in significant film variance. On the other hand, in closed-loop depositions, as demonstrated in the simula-

tion, feedback control is able to effectively compensate for the stochasticity of the process and, therefore, significantly reduce the film variance and outperform the recipe-based open-loop deposition.

5. Conclusions

In this work, we focused on a thin film deposition process which took place on a 2D lattice and was governed by three microscopic processes including molecule adsorption, surface migration, and desorption. A 2D linear stochastic PDE model was initially constructed, following the methodology proposed in our previous work,²³ which describes the spatio-temporal evolution of the film surface. Then, the control problem was formulated as the one of regulating the thin film thickness and surface roughness by manipulating the substrate temperature and adsorption rate. Subsequently, a computationally efficient multivariable predictive control algorithm was developed which used a finite-dimensional approximation of the stochastic PDE model to regulate the thin film thickness and surface roughness at desired levels at the end of the deposition. The predictive controller was then applied to the kMC simulation of the deposition process. Closed-loop system simulation results demonstrated that the model was adequately accurate and that the controller was effective in enforcing the desired control objectives and reducing the film variance caused by the stochasticity of the growth process.

Acknowledgment

Financial support for this work from the NSF (ITR), CTS-0325246, is gratefully acknowledged.

Literature Cited

- Theodoropoulou, A.; Adomaitis, R. A.; Zafiriou, E. Inverse model based real-time control for temperature uniformity of RTCVD. *IEEE Trans. Semiconduct. Manufact.* **1999**, *12*, 87–101.
- Christofides, P. D. *Nonlinear and Robust Control of Partial Differential Equation Systems: Methods and Applications to Transport-Reaction Processes*; Birkhäuser: Boston, 2001.
- Armaou, A.; Christofides, P. D. Plasma-enhanced chemical vapor deposition: Modeling and control. *Chem. Eng. Sci.* **1999**, *54*, 3305–3314.
- Ni, D.; Lou, Y.; Christofides, P. D.; Sha, L.; Lao, S.; Chang, J. P. Real-time carbon content control for PECVD ZrO₂ thin film growth. *IEEE Trans. Semiconduct. Manufact.* **2004**, *17*, 221–230.
- Gillespie, D. T. A general method for numerical simulating the stochastic time evolution of coupled chemical reactions. *J. Comput. Phys.* **1976**, *22*, 403–434.
- Fichthorn, K. A.; Weinberg, W. H. Theoretical foundations of dynamic Monte Carlo simulations. *J. Chem. Phys.* **1991**, *95*, 1090–1096.
- Katsoulakis, M. A.; Majda, A. J.; Vlachos, D. G. Coarse-grained stochastic processes and Monte Carlo simulations in lattice systems. *J. Comput. Phys.* **2003**, *186*, 250–278.
- Edwards, S. F.; Wilkinson, D. R. The surface statistics of a granular aggregate. *Proc. R. Soc. London, Ser. A* **1982**, *381*, 17–31.
- Vvedensky, D. D.; Zangwill, A.; Luse, C. N.; Wilby, M. R. Stochastic equations of motion for epitaxial growth. *Phys. Rev. E* **1993**, *48*, 852–862.
- Lou, Y.; Christofides, P. D. Estimation and control of surface roughness in thin film growth using kinetic Monte Carlo models. *Chem. Eng. Sci.* **2003**, *58*, 3115–3129.
- Lou, Y.; Christofides, P. D. Feedback control of growth rate and surface roughness in thin film growth. *AIChE J.* **2003**, *49*, 2099–2113.
- Lou, Y.; Christofides, P. D. Feedback control of surface roughness of GaAs (001) thin films using kinetic Monte Carlo models. *Comput. Chem. Eng.* **2005**, *29*, 225–241.

(13) Ni, D.; Christofides, P. D. Dynamics and control of thin film surface microstructure in a complex deposition process. *Chem. Eng. Sci.* **2005**, *60*, 1603–1617.

(14) Gallivan, M. A.; Murray, R. M. Reduction and identification methods for Markovian control systems, with application to thin film deposition. *Int. J. Robust Nonlin. Control* **2004**, *14*, 113–132.

(15) Siettos, C. I.; Armaou, A.; Makeev, A. G.; Kevrekidis, I. G. Microscopic/stochastic timesteppers and “coarse” control: A KMC example. *AIChE J.* **2003**, *49*, 1922–1926.

(16) Armaou, A.; Siettos, C. I.; Kevrekidis, I. G. Time-steppers and “coarse” control of distributed microscopic processes. *Int. J. Robust Nonlin. Control* **2004**, *14*, 89–111.

(17) Lauritsen, K. B.; Cuerno, R.; Makse, H. A. Noisy Kuramoto-Sivashinsky equation for an erosion model. *Phys. Rev. E* **2003**, *54*, 3577–3580.

(18) Lou, Y.; Christofides, P. D. Feedback control of surface roughness using stochastic PDEs. *AIChE J.* **2005**, *51*, 345–352.

(19) Lou, Y.; Christofides, P. D. Feedback control of surface roughness in sputtering processes using the stochastic Kuramoto-Sivashinsky equation. *Comput. Chem. Eng.*, in press.

(20) Marsili, M.; Maritan, A.; Toigo, F.; Banavar, J. R. Stochastic growth equations and reparametrization invariance. *Rev. Mod. Phys.* **1996**, *68*, 963–983.

(21) Park, S.; Kim, D.; Park, J. Derivation of continuum stochastic equations for discrete growth models. *Phys. Rev. E* **2002**, *65*, 015102(R).

(22) Vvedensky, D. D. Edwards-Wilkinson equation from lattice transition rules. *Phys. Rev. E* **2003**, *67*, 025102(R).

(23) Ni, D.; Christofides, P. D. Construction of stochastic PDEs for feedback control of surface roughness in thin film deposition. *Int. J. Robust Nonlin. Control*, submitted; a short version of this work will appear in the Proceedings of the 2005 American Control Conference.

(24) Shitara, T.; Vvedensky, D. D.; Wilby, M. R.; Zhang, J.; Neave, J. H.; Joyce, B. A. Step-density variations and reflection high-energy electron-diffraction intensity oscillations during epitaxial growth on vicinal GaAs(001). *Phys. Rev. B* **1992**, *46*, 6815–6824.

(25) Vlachos, D. G. Multiscale integration hybrid algorithms for homogeneous–heterogeneous reactors. *AIChE J.* **1997**, *43*, 3031.

(26) Åström, K. J. *Introduction to Stochastic control Theory*; Academic Press: New York, 1970.

(27) Taylor, M. E.; Atwater, H. A. Monte Carlo simulations of epitaxial growth: Comparison of pulsed laser deposition and molecular beam epitaxy. *Appl. Surf. Sci.* **1998**, *127*, 159–163.

(28) Amar, J. G.; Family, F. Deterministic and stochastic surface growth with generalized nonlinearity. *Phys. Rev. E* **1993**, *47*, 1595–1603.

(29) Eierdal, L.; Besenbacher, F.; Laegsgaard, E.; Stensgaard, I. Interaction of oxygen with Ni(110) studied by scanning tunneling microscopy. *Surf. Sci.* **1994**, *312*, 31–53.

(30) Lee, K. L.; Hu, C. K.; Tu, K. N. In situ scanning electron microscope comparison studies on electromigration of Cu and Cu(Sn) alloys for advanced chip interconnects. *J. Appl. Phys.* **1995**, *78*, 4428–4437.

(31) Reviakine, I.; Brisson, A. Formation of supported phospholipid bilayers from unilamellar vesicles investigated by atomic force microscopy. *Langmuir* **2000**, *16*, 1806–1815.

(32) Renaud, G.; Lazzari, R.; Revenant, C.; Barbier, A.; Noblet, M.; Ulrich, O.; Leroy, F.; Jupille, J.; Borensztein, Y.; Henry, C. R.; Deville, J. P.; Scheurer, F.; Mane-Mane, J. Real-time monitoring of growing nanoparticles. *Science* **2003**, *300*, 1416–1419.

(33) Christofides, P. D.; Daoutidis, P. Finite-dimensional control of parabolic PDE systems using approximate inertial manifolds. *J. Math. Anal. Appl.* **1997**, *216*, 398–420.

(34) Baker, J.; Christofides, P. D. Finite dimensional approximation and control of nonlinear parabolic PDE systems. *Int. J. Contr.* **2000**, *73*, 439–456.

(35) Fletcher, R. *Practical methods of optimization*, 2nd ed.; John Wiley & Sons: New York, 1987.

Received for review September 28, 2004

Revised manuscript received December 7, 2004

Accepted December 10, 2004

IE049051L